Article

Cell Metabolism

Activation of Cardiac Fibroblast Growth Factor Receptor 4 Causes Left Ventricular Hypertrophy

Graphical Abstract

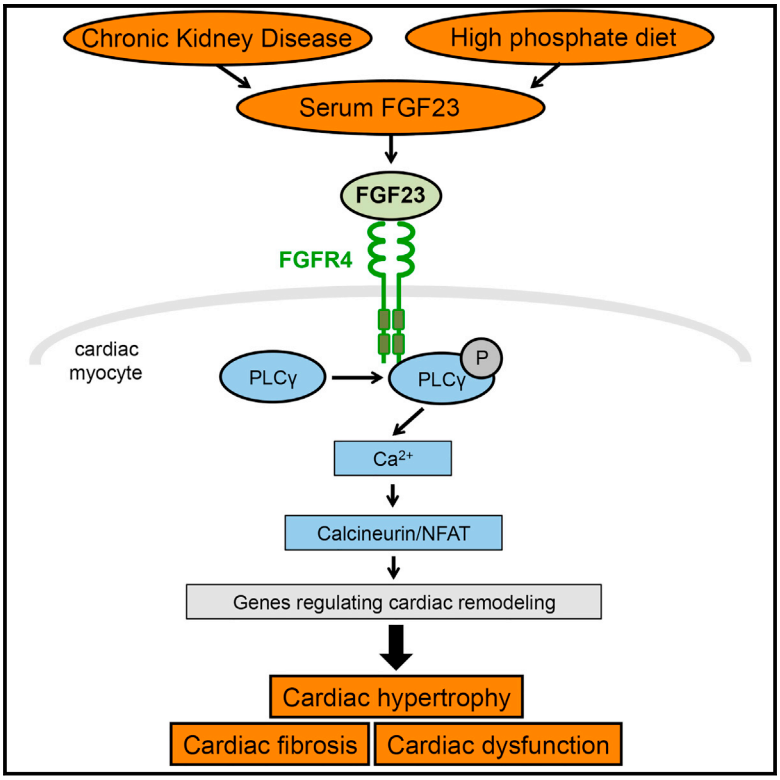

Highlights

- In the absence of α-klotho, FGF23 induces binding of FGFR4 to PLCγ
- FGF23 activates calcineurin/NFAT signaling in cardiac myocytes via FGFR4
- FGFR4 blockade protects CKD rats with high serum FGF23 from cardiac hypertrophy
- Knockin mice carrying a FGFR4 gain-of-function mutation develop cardiac hypertrophy

Authors

Alexander Grabner, Ansel P. Amaral, Karla Schramm, ..., Marcus Brand, Myles Wolf, Christian Faul

Correspondence

cfaul@med.miami.edu

In Brief

Grabner et al. reveal that FGFR4 mediates the pro-hypertrophic cardiac effects of FGF23, a phosphate-regulating hormone elevated in patients with chronic kidney disease (CKD). Activation of FGFR4/calcineurin/NFAT signaling is sufficient to induce cardiac hypertrophy in mice, while FGFR4 blockade attenuates cardiac hypertrophy in a rat model of CKD.

Grabner et al., 2015, Cell Metabolism 22, 1020–1032
December 1, 2015
http://dx.doi.org/10.1016/j.cmet.2015.09.002

CellPress

Cell Metabolism
Article

Activation of Cardiac Fibroblast Growth Factor Receptor 4 Causes Left Ventricular Hypertrophy

Alexander Grabner,[1,13] Ansel P. Amaral,[1,2,13] Karla Schramm,[1,2] Saurav Singh,[1,2] Alexis Sloan,[1,2] Christopher Yanucil,[1,2] Jihe Li,[3,4] Lina A. Shehadeh,[3,4,5] Joshua M. Hare,[3,4] Valentin David,[1,6] Aline Martin,[1,6] Alessia Fornoni,[1] Giovana Seno Di Marco,[7] Dominik Kentrup,[7] Stefan Reuter,[7] Anna B. Mayer,[7] Hermann Pavenstädt,[7] Jörg Stypmann,[8] Christian Kuhn,[9] Susanne Hille,[9] Norbert Frey,[9] Maren Leifheit-Nestler,[10] Beatrice Richter,[10] Dieter Haffner,[10] Reimar Abraham,[11] Johannes Bange,[11] Bianca Sperl,[12] Axel Ullrich,[12] Marcus Brand,[7] Myles Wolf,[6] and Christian Faul[1,2,*]

[1]Katz Family Drug Discovery Center and Division of Nephrology and Hypertension, Department of Medicine, University of Miami Leonard M. Miller School of Medicine, Miami, FL 33136, USA

[2]Department of Cell Biology and Anatomy, University of Miami Leonard M. Miller School of Medicine, Miami, FL 33136, USA

[3]Interdisciplinary Stem Cell Institute, University of Miami Leonard M. Miller School of Medicine, Miami, FL 33136, USA

[4]Division of Cardiology, Department of Medicine, University of Miami Leonard M. Miller School of Medicine, Miami, FL 33136, USA

[5]Vascular Biology Institute, University of Miami Leonard M. Miller School of Medicine, Miami, FL 33136, USA

[6]Division of Nephrology and Hypertension, Department of Medicine and Center for Translational Metabolism and Health, Institute for Public Health and Medicine, Northwestern University Feinberg School of Medicine, Chicago, IL 60611, USA

[7]Department of Internal Medicine D, University Hospital Münster, 48149 Münster, Germany

[8]Division of Cardiology, Department of Cardiovascular Medicine, University Hospital Münster, 48149 Münster, Germany

[9]Department of Cardiology and Angiology, University Medical Center of Schleswig-Holstein, Campus Kiel, 24105 Kiel, Germany

[10]Department of Pediatric Kidney, Liver and Metabolic Diseases, Hannover Medical School, 30625 Hannover, Germany

[11]U3 Pharma GmbH, 82152 Martinsried, Germany

[12]Department of Molecular Biology, Max Planck Institute of Biochemistry, 82152 Martinsried, Germany

[13]Co-first author

*Correspondence: cfaul@med.miami.edu

http://dx.doi.org/10.1016/j.cmet.2015.09.002

SUMMARY

Chronic kidney disease (CKD) is a worldwide public health threat that increases risk of death due to cardiovascular complications, including left ventricular hypertrophy (LVH). Novel therapeutic targets are needed to design treatments to alleviate the cardiovascular burden of CKD. Previously, we demonstrated that circulating concentrations of fibroblast growth factor (FGF) 23 rise progressively in CKD and induce LVH through an unknown FGF receptor (FGFR)-dependent mechanism. Here, we report that FGF23 exclusively activates FGFR4 on cardiac myocytes to stimulate phospholipase Cγ/calcineurin/nuclear factor of activated T cell signaling. A specific FGFR4-blocking antibody inhibits FGF23-induced hypertrophy of isolated cardiac myocytes and attenuates LVH in rats with CKD. Mice lacking FGFR4 do not develop LVH in response to elevated FGF23, whereas knockin mice carrying an FGFR4 gain-of-function mutation spontaneously develop LVH. Thus, FGF23 promotes LVH by activating FGFR4, thereby establishing FGFR4 as a pharmacological target for reducing cardiovascular risk in CKD.

INTRODUCTION

Chronic kidney disease (CKD) is a global public health problem that shortens lifespan, primarily by increasing risk of cardiovascular disease (Eckardt et al., 2013). Novel therapeutic targets are urgently needed to reduce the burden of cardiovascular disease in CKD.

Left ventricular hypertrophy (LVH) is a common pattern of cardiovascular injury in CKD that affects up to 75% of individuals by the time they reach end-stage renal disease (Faul et al., 2011). By promoting heart failure and atrial and ventricular arrhythmias, LVH is a powerful risk factor for cardiovascular events and death (de Simone et al., 2008). The complex pathogenesis of LVH involves ventricular pressure and volume overload, but emerging data also implicate a novel role for the bone-derived, phosphate-regulating hormone fibroblast growth factor (FGF) 23 (Gutiérrez et al., 2009).

The primary physiological effects of FGF23 to stimulate urinary phosphate excretion and reduce circulating calcitriol concentrations are mediated by FGF23 binding to FGF receptors (FGFR) in the kidney, with α-klotho serving as the co-receptor that enhances binding affinity (Urakawa et al., 2006). Serum levels of FGF23 rise progressively as kidney function declines, presumably as a compensation to maintain neutral phosphate balance in the setting of reduced glomerular filtration of phosphate (Wolf, 2012). However, chronically elevated FGF23 levels may be ultimately maladaptive in patients with CKD, given the powerful dose-dependent associations of higher FGF23 with increased risks of LVH, congestive heart failure, and death (Gutiérrez et al., 2008, 2009; Isakova et al., 2011).

FGF23 induces hypertrophic growth of cardiac myocytes in vitro and LVH in rodents through a direct FGFR-dependent mechanism, but independently of α-klotho, which is not expressed in cardiac myocytes (Faul et al., 2011). Whereas α-klotho-expressing cells in the kidney respond to FGF23 by activating the Ras/mitogen-activated protein kinase (MAPK) cascade

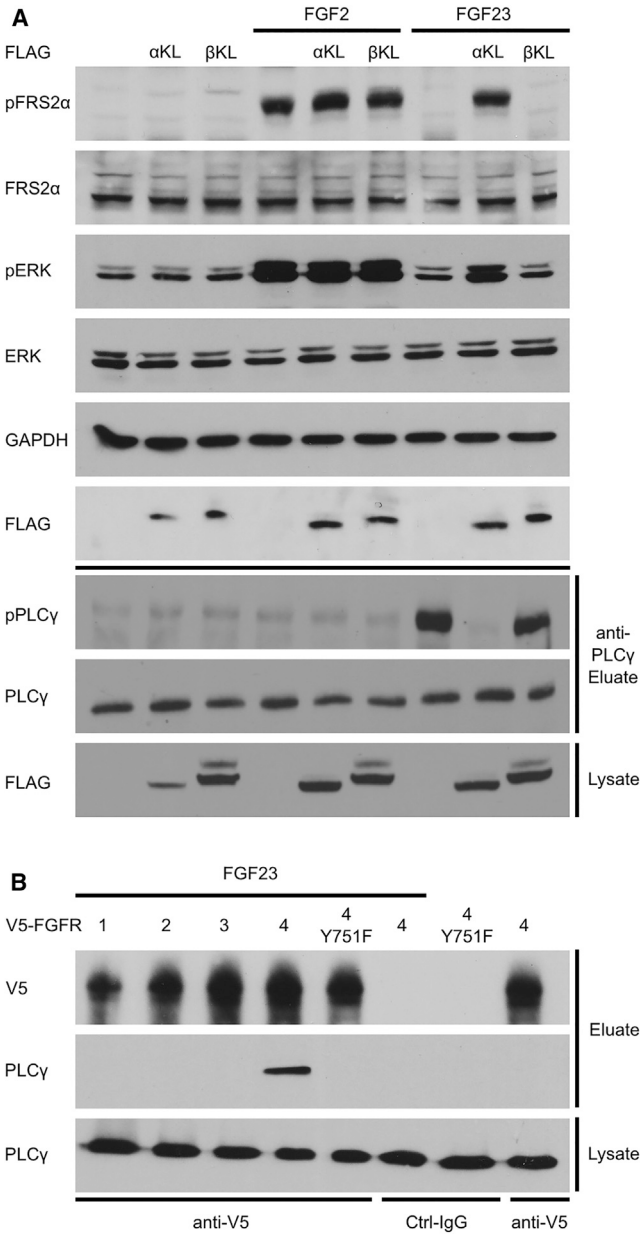

Figure 1. FGF23 Activates FGFR4 and PLCγ Signaling in HEK293 Cells

(A) FGF23 treatment increases levels of phosphorylated PLCγ in HEK293 cells within 30 min, as revealed by immunoprecipitation of endogenous PLCγ and western blot analysis of eluates with anti-phospho-PLCγ. FGF23 does not increase phosphorylation of FRS2α or ERK1/2, as shown by western blot analyses of total protein extracts. In contrast, FGF23 induces phosphorylation of FRS2α and ERK1/2, but not PLCγ, in cells that overexpress FLAG-tagged α-klotho (αKL). HEK293 cells that overexpress β-klotho (βKL) respond to FGF23 similar to untransfected cells. FGF2 induces phosphorylation of FRS2α and ERK1/2, regardless of presence of α- or β-klotho. Overexpression of FLAG-tagged α- or β-klotho does not induce phosphorylation of FRS2α, ERK1/2, or PLCγ in the absence of FGF treatment. GAPDH serves as loading control.

(B) The four different FGFR isoforms (c splice variants of FGFR1–3) were overexpressed as V5-tagged fusion proteins in HEK293 cells for 2 days, serum starved overnight, and treated with FGF23 for 30 min followed by anti-V5 immunoprecipitation from total protein extracts. Endogenous PLCγ co-precipitates only with FGFR4. In the absence of FGF23 treatment or if the FGFR4-Y751F mutant form is overexpressed, PLCγ cannot be detected in the eluate. Immunoprecipitations with control antibody (Ctrl-IgG) do not result in purification of V5-FGFR4 or PLCγ.

See also Figure S1.

(Urakawa et al., 2006), the pro-hypertrophic effects of FGF23 on cardiac myocytes were blocked by pharmacologic inhibition of phospholipase Cγ (PLCγ) and calcineurin (Faul et al., 2011). In contrast, the pro-hypertrophic effects of the prototypical paracrine FGF family member, FGF2, were blocked by inhibitors of the Ras/MAPK cascade (Faul et al., 2011). These findings suggest that different FGF ligands can activate distinct downstream signaling pathways in cardiac myocytes and that in the absence of α-klotho, FGF23 activates the PLCγ/calcineurin/nuclear factor of activated T cell (NFAT) signaling axis, which is a potent inducer of pathological LVH (Molkentin et al., 1998). However, the identity of the specific FGFR that mediates the cardiac effects of FGF23 is unknown.

The mammalian genome encodes four FGFR isoforms, FGFR1–4, that are receptor tyrosine kinases (Ornitz and Itoh, 2001). Following ligand-induced auto-phosphorylation of FGFR, FGF receptor substrate (FRS) 2α undergoes tyrosine phosphorylation by FGFR and stimulates Ras/MAPK and PI3K/Akt signaling (Eswarakumar et al., 2005). In contrast to FRS2α, which is constitutively bound to FGFR independent of the receptor's activation state, PLCγ can also be recruited to bind directly to one specific phosphorylated tyrosine residue (pY751 in mouse FGFR4) within a consensus sequence (YLDL) in the FGFR cytoplasmic tail (Mohammadi et al., 1991; Vainikka et al., 1994). Subsequent phosphorylation of PLCγ by FGFR activates PLCγ (Burgess et al., 1990), which induces generation of diacylglycerol and inositol 1,4,5-triphosphate, and increases cytoplasmic Ca^{2+}, which activates calcineurin and its substrate, NFAT (Eswarakumar et al., 2005). Here, we report our investigation into the specific FGFR isoform that mediates PLCγ signaling and the pro-hypertrophic effects of FGF23 in cardiac myocytes.

RESULTS

FGF23 Activates FGFR4 and PLCγ Signaling in the Absence of α-Klotho

To study FGF-FGFR-dependent signaling, we used HEK293 cells that express all FGFR isoforms but lack α-klotho (data not shown), similar to cardiac myocytes (Faul et al., 2011). As a read-out of calcineurin/NFAT versus Ras/MAPK activation, we analyzed phosphorylation of PLCγ and FRS2α. In response to 30 min of treatment, FGF23 increased phosphorylated PLCγ levels without changing overall PLCγ expression, but did not induce phosphorylation of FRS2α (Figure 1A). In contrast, FGF2 had no effect on phospho-PLCγ levels but increased phosphorylation of FRS2α and ERK1/2. Thus, in HEK293 cells, FGF23 and FGF2 activate distinct FGFR adaptor proteins, which could explain their differential downstream signaling in cardiac myocytes (Faul et al., 2011).

To test if the presence of α-klotho determines whether FGF23 activates FGFR-mediated downstream signaling by PLCγ/calcineurin/NFAT or FRS2α/Ras/MAPK, we introduced ectopic α-klotho into HEK293 cells. Subsequent FGF23 treatment increased

phosphorylation of FRS2α and ERK1/2, but did not activate PLCγ (Figure 1A), similar to the response of non-transfected HEK293 cells to FGF2. In contrast, when we overexpressed ectopic β-klotho that does not bind FGF23 (Ogawa et al., 2007), FGF23 induced phosphorylation of PLCγ (Figure 1A). As expected, given its lack of reliance on klotho (Goetz et al., 2012), FGF2-mediated FRS2α/Ras/MAPK signaling was unaffected by the presence or absence of α-klotho or β-klotho. These data indicate that in the absence of α-klotho, FGF23-induced FGFR activation stimulates PLCγ signaling, whereas overexpression of α-klotho causes a signaling switch to the Ras/MAPK cascade, similar to cells that endogenously express α-klotho (Urakawa et al., 2006).

To determine which FGFR isoforms are activated by FGF23 in the absence of α-klotho, we analyzed FGFR binding to PLCγ in response to FGF23 treatment. HEK293 cells were transfected with V5-tagged FGFR1, FGFR2, FGFR3, or FGFR4 and incubated with FGF23 or PBS as negative control. After 30 min, we immunoprecipitated the FGFR isoforms from lysates with anti-V5 and tested for co-precipitation of PLCγ by immunoblot analysis of eluates. Among the FGFR isoforms, only FGFR4 bound PLCγ in response to FGF23 treatment (Figure 1B). We also overexpressed a V5-tagged murine FGFR4 cDNA carrying a tyrosine to phenylalanine substitution at residue 751 (FGFR4-Y751F) that cannot be phosphorylated and therefore cannot activate PLCγ upon ligand stimulation (Vainikka et al., 1994). In contrast to wild-type FGFR4, FGFR4-Y751F did not co-precipitate PLCγ upon FGF23 treatment (Figure 1B). Although FGFR1, FGFR3, and FGFR4 can act as FGF23 receptors in α-klotho expressing cells (Kurosu et al., 2006), our results indicate that in the absence of α-klotho, FGF23 can stimulate FGFR4-dependent signaling by specifically activating PLCγ via phosphorylation of FGFR4 at Y751.

FGF23 Activates FGFR4 and PLCγ Signaling in Cultured Cardiac Myocytes

To test whether FGFR4 could function as a FGF23 receptor in cardiac myocytes, we first analyzed FGFR4 protein expression in the murine heart with constitutive FGFR4 knockout (*FGFR4*$^{-/-}$) mice used as negative control (Weinstein et al., 1998). Immunoprecipitation and western blot analyses of protein extracts from total hearts and isolated neonatal mouse ventricular myocytes (NMVM) from wild-type mice revealed a signal with the expected size of FGFR4 (approximately 110 kDa) (Partanen et al., 1991) that was absent in extracts from *FGFR4*$^{-/-}$ mice (Figure 2A). Immunocytochemical analysis confirmed that FGFR4 is expressed in wild-type, but not *FGFR4*$^{-/-}$, NMVM (Figure 2B). Flow cytometry analysis of the adult mouse heart indicated that FGFR4 is expressed by cardiac myocytes and absent from non-myocytes (Figure 2C). Immunohistochemical analysis of fresh human heart samples confirmed that FGFR4 protein is also expressed in human cardiac myocytes (Figures 2D and 2E).

To determine if FGF23 can activate FGFR4 in cardiac myocytes, we analyzed binding of PLCγ to FGFR4 in isolated neonatal rat ventricular myocytes (NRVM) that were treated for 30 min with FGF23 or FGF2 as negative control. We immunoprecipitated endogenous PLCγ from total protein extracts and analyzed eluates by immunoblotting with antibodies against FGFR4. Compared to eluates derived from control cells that were incubated with PBS or FGF2, levels of co-purified FGFR4 were elevated in FGF23-treated NRVM, while total FGFR4 and PLCγ expression levels were unchanged (Figure 3A). In contrast, when cells were co-treated with an isoform-specific antibody that blocks FGFR4 exclusively among the FGFR isoforms and their splice variants (anti-FGFR4; Figures S3A and S3B), levels of PLCγ-bound FGFR4 were not elevated in comparison to control cells.

To determine if FGF23 could activate calcineurin/NFAT signaling further downstream, we studied FGF23 effects on the transcriptional activity of NFAT in NRVM. We conducted chemiluminescence reporter assays in NRVM that were transduced with a cDNA construct encoding for firefly luciferase under the control of three NFAT binding elements. After 2 hr of treatment, FGF23 caused a significant elevation in luciferase activity that was blocked by the calcineurin inhibitor, cyclosporine A (Figure 3B). In contrast, FGF2 did not increase luciferase activity. This result is consistent with our previous finding that cyclosporine A could block FGF23-induced, but not FGF2-induced, hypertrophy of NRVM (Faul et al., 2011). To study if FGF23-induced NFAT activation is mediated by FGFR4, we treated luciferase reporter NRVM with FGF23 and anti-FGFR4 or AZD4547, a small-molecule inhibitor of FGFR with greater affinity for FGFR1–3 versus FGFR4. Anti-FGFR4, but not AZD4547, blocked FGF23-induced elevation in luciferase activity (Figure 3B).

Next, we treated NRVM with FGF23 or FGF2 for 30 min and determined activation of the Ras/MAPK signaling pathway by western blot analysis of total protein extracts. Consistent with our previous findings (Faul et al., 2011), FGF2, but not FGF23, increased levels of phosphorylated FRS2α and ERK1/2 (Figure 3C), and anti-FGFR4 did not block FGF2-induced phosphorylation of FRS2α and ERK1/2 (Figure 3C).

Overall, our findings in cultured cardiac myocytes parallel our results in HEK293 cells and indicate that in the absence of α-klotho, FGF23 activates FGFR4, resulting in recruitment of PLCγ to the receptor and activation of calcineurin/NFAT signaling. In contrast, FGF2 activates Ras/MAPK signaling in NRVM independently of FGFR4.

FGFR4 Mediates FGF23-Induced Hypertrophy of Cardiac Myocytes In Vitro

To determine if FGFR4 mediates the pro-hypertrophic effects of FGF23, NRVM were co-treated with FGF23 or FGF2 and a series of receptor antagonists for 48 hr. The anti-FGFR4 blocking antibody reduced FGF23-induced, but not FGF2-induced, hypertrophy (Figures 4A and 4B). The pan-FGFR blocker, PD173074, inhibited the effects of both FGF2 and FGF23, whereas the FGFR1–3 inhibitor, AZD4547, prevented FGF2-induced, but not FGF23-induced, hypertrophy (Figure 4B).

Consistent with our immunocytochemistry findings, both FGF23 and FGF2 significantly increased expression of the markers of cardiac hypertrophy, atrial, and brain natriuretic peptide (ANP, BNP), whereas pan-FGFR inhibition blocked these effects (Figure 4C). In contrast, anti-FGFR4 specifically inhibited FGF23-mediated increases in ANP and BNP expression, indicating that these pro-hypertrophic effects of FGF23 on NRVM require FGFR4 activation.

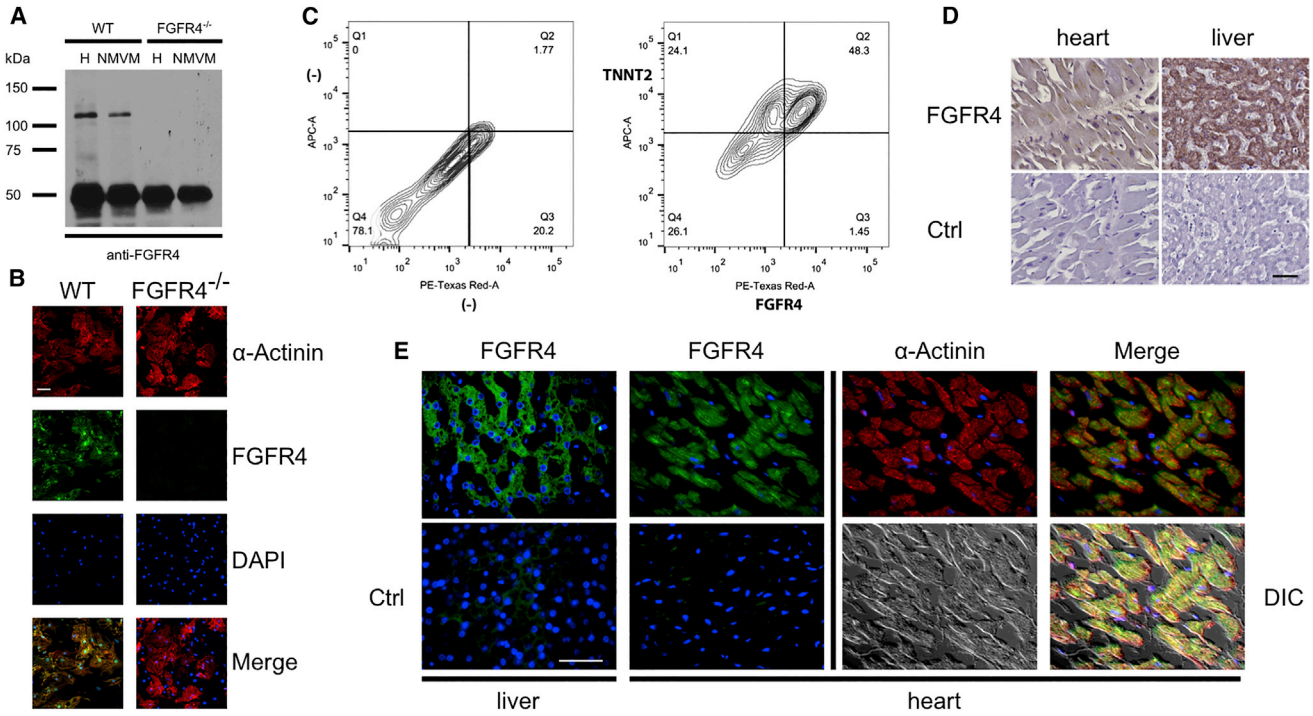

Figure 2. FGFR4 Is Expressed in Cardiac Myocytes

(A) Immunoprecipitation of FGFR4 from total heart tissue (H) and isolated ventricular myocytes of newborn wild-type and FGFR4 knockout (*FGFR4*$^{-/-}$) mice (NMVM) followed by immunoblotting for FGFR4 reveals the expected 110-kDa signal of FGFR4 in wild-type, but not *FGFR4*$^{-/-}$, mice. The 50-kDa signal is the IgG heavy chain of anti-FGFR4.

(B) Immunocytochemical analysis shows a striated localization pattern of FGFR4 (red) in wild-type NMVM that is absent in *FGFR4*$^{-/-}$ cells. In wild-type NMVM, FGFR4 is present only in cardiac myocytes, but not other co-purified cells, as evident by FGFR4 labeling of α-actinin expressing cells (green). DAPI (blue) identifies nuclei (original magnification, ×40; scale bar, 50 μm).

(C) Representative dot blots of three independent flow cytometric analyses of single cell suspensions from adult wild-type mouse hearts. Labeling without primary antibodies is used as negative control (–). Numbers refer to percentages of quadrant analysis. FGFR4 is present in cardiac troponin-T (TNNT2)-positive myocytes, whereas TNNT2-negative non-myocytes show no FGFR4 labeling.

(D) Immunoperoxidase labeling of fresh human cardiac tissue with anti-FGFR4 shows a positive signal that is absent if only secondary antibody is used (Ctrl). As positive control, human liver tissue shows high levels of FGFR4 expression.

(E) Immunohistochemical analysis of human cardiac tissue with anti-FGFR4 (green) shows labeling of the myocardium, as visualized by differential interference contrast (DIC), and of cardiac myocytes, as identified by co-labeling with anti-α-actinin (red). Fluorochrome-conjugated secondary antibody only was used as negative control (Ctrl). DAPI (blue) shows nuclei. As positive control, anti-FGFR4 shows strong immunolabeling of hepatocytes in human liver tissue.

See also Figure S2.

In support of this finding, 48 hr of treatment with FGF23 induced an increase in cross-sectional area of wild-type NMVM, but not NMVM from *FGFR4*$^{-/-}$ mice (Figures 4D and 4E). In contrast, FGF2 and the pro-hypertrophic angiotensin (Ang) II induced hypertrophic growth of NMVM independently of FGFR4. In wild-type NMVM, FGF23, FGF2, and AngII all increased expression of β-myosin heavy chain (β-MHC) protein, which is a fetal MHC isoform that is upregulated in cardiac hypertrophy (Izumo et al., 1987), but only FGF2 and AngII induced this effect in *FGFR4*$^{-/-}$ NMVM (Figures 4F and 4G). These data indicate that the pro-hypertrophic effects of FGF23 in cultured cardiac myocytes require FGFR4.

FGFR4 Loss of Function Protects Mice with Elevated FGF23 from LVH

To determine if FGFR4 mediates FGF23-induced LVH in vivo, we elevated endogenous serum FGF23 levels in wild-type and constitutive *FGFR4*$^{-/-}$ mice by administering 12 weeks of a high phosphate (2%) diet that is known to induce LVH (Hu et al., 2015). Serum phosphate and FGF23 levels increased significantly in both wild-type and *FGFR4*$^{-/-}$ mice in the absence of changes in kidney function (Figures 5A–5C). In response to high phosphate diet, wild-type mice developed LVH, marked by increases in left ventricular (LV) wall thickness, cross-sectional area of individual cardiac myocytes, and myocardial fibrosis (Figures 5D–5G). In contrast, *FGFR4*$^{-/-}$ mice did not develop LVH or fibrosis despite their similar degree of FGF23 elevation (Figures 5D–5G). High phosphate diet increased cardiac levels of phosphorylated PLCγ and expression of regulator of calcineurin 1 (RCAN1), an established NFAT target gene (Yang et al., 2000), in wild-type mice but not in *FGFR4*$^{-/-}$ mice (Figures S5A and S5B). We conclude that FGFR4 is required for activation of cardiac PLCγ/calcineurin/NFAT signaling and development of LVH and myocardial fibrosis in mice with high serum FGF23 levels.

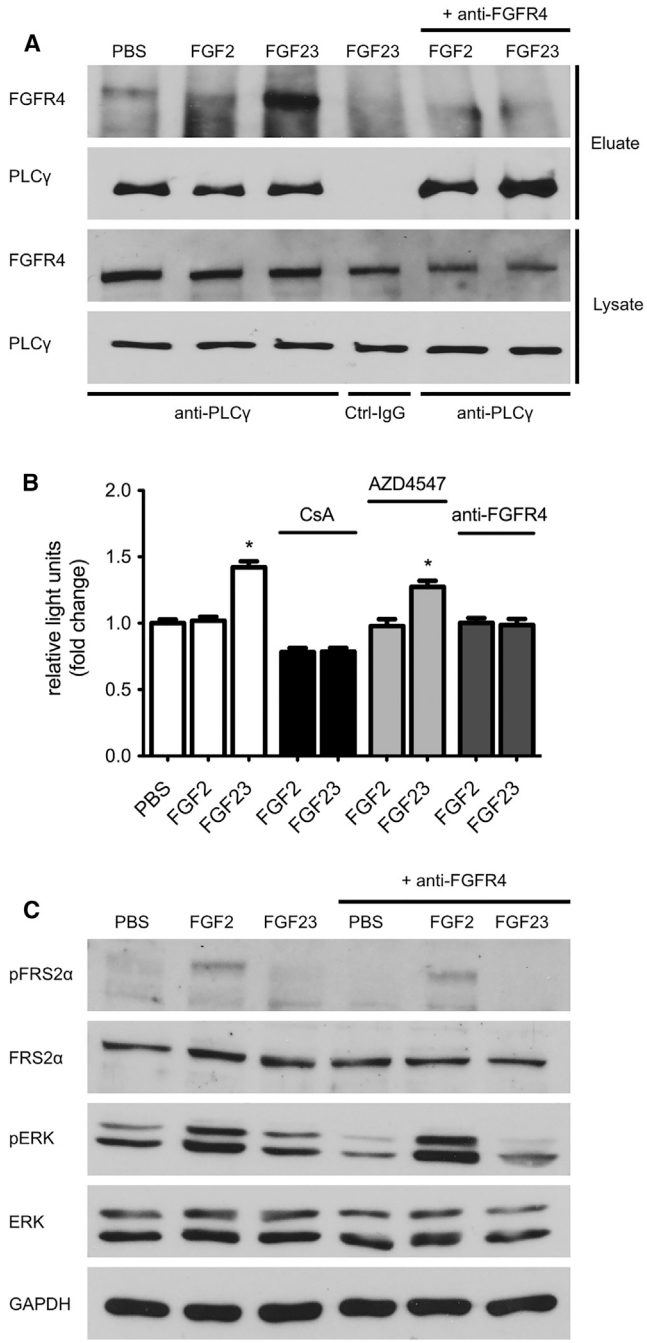

Figure 3. FGF23 Activates FGFR4 in Cultured Cardiac Myocytes

(A) NRVM were co-treated with FGF23 or FGF2 and a FGFR4 blocking antibody (anti-FGFR4) for 30 min followed by anti-PLCγ immunoprecipitation from total protein extracts. The amount of co-precipitated FGFR4 is increased in cells that were treated with FGF23 compared to FGF2-treated or untreated cells. In the presence of anti-FGFR4, levels of FGFR4 in anti-PLCγ eluates are reduced. Immunoprecipitation with control antibody (Ctrl-IgG) does not result in purification of PLCγ or FGFR4.

(B) FGF23 treatment of NFAT-luciferase reporter NRVM for 2 hr significantly increases luciferase activity compared to vehicle- and FGF2-treated cells. The effect is blocked in cells that were co-treated with cyclosporine A (CsA) or anti-FGFR4, but not with the FGFR1–3 inhibitor, AZD4547. Values represent fold change in relative light units ± SEM compared with vehicle treated cells; *$p < 0.0001$.

(C) NRVM were treated with FGF23 or FGF2 for 30 min followed by immunoblot analysis of total protein extracts. Only FGF2 causes an increase in levels of phospho-FRS2α and phospho-ERK. This effect is not reduced in the presence of anti-FGFR4. GAPDH serves as loading control.

See also Figure S3.

FGFR4 Blockade Attenuates LVH in the 5/6 Nephrectomy Rat Model of CKD

We tested the therapeutic potential of interfering with cardiac FGF23-FGFR4 signaling in the 5/6 nephrectomy rat model of CKD that develops increased FGF23 levels, severe hypertension, and LVH within 14 days after nephrectomy (Faul et al., 2011). We administered the specific anti-FGFR4 blocking antibody (25 mg/kg body weight via intraperitoneal injection) beginning 1 hr after nephrectomy and then every 3 days through day 12. At day 14 after nephrectomy, renal function was significantly impaired and blood pressure and serum FGF23 levels significantly elevated in the animals that underwent 5/6 versus sham nephrectomy, but there were no significant differences between 5/6 nephrectomized animals that received anti-FGFR4 antibodies or PBS (Table S1). Compared to PBS-treated 5/6 nephrectomized rats, treatment with anti-FGFR4 antibody significantly attenuated LVH and myocardial fibrosis, as demonstrated by significant decreases in ratio of heart weight to tibia length, LV mass, LV wall thickness, cross-sectional area of individual cardiac myocytes, and collagen fiber content (Figures 6A–6F). Consistent with our histological findings, expression analyses for markers of cardiac hypertrophy and fibrosis confirmed the protective effects of anti-FGFR4 (Figures 6G and 6H). Echocardiographic analyses revealed no significant systolic changes in ejection fraction among the three groups (Figure 6I). However, compared with vehicle-treated 5/6 nephrectomzied rats, anti-FGFR4 treatment significantly improved diastolic function (Figure 6J). Anti-FGFR4 treatment attenuated the 5/6 nephrectomy-induced increase in cardiac expression levels of the NFAT target genes, RCAN1 and transient receptor potential channel 6 (TRPC6; Figures S5C and S5D). These data indicate that blocking FGFR4 inhibits cardiac calcineurin/NFAT signaling and attenuates the development of LVH and cardiac fibrosis in a well-established animal model of CKD without significantly altering kidney function, blood pressure, or FGF23 levels.

Constitutive FGFR4 Activation Causes LVH in Mice

Gain-of-function mutations in human FGFR4 are associated with malignancy (Bange et al., 2002). In the *FGFR4Arg388* allele, replacing a neutral glycine with a charged arginine residue in the transmembrane domain increases protein stability and prolongs phosphorylation of FGFR4 (Wang et al., 2008). Knockin mice with the murine homolog, *FGFR4Arg385*, show advanced tumor development and accelerated metastasis when exposed to carcinogens (Seitzer et al., 2010). We hypothesized that expression of *FGFR4Arg385* predisposes to cardiac hypertrophy. As reported previously (Seitzer et al., 2010), FGFR4 expression is unchanged in the heart of homozygous knockin mice (*FGFR4Arg/Arg385*) compared to wild-type (*FGFR4Gly/Gly385*). However, unlike wild-type littermates, 6-month-old *FGFR4Arg/Arg385* mice demonstrated LVH, as indicated by significant increases in heart weight, LV wall thickness, cross-sectional area of individual cardiac myocytes, and cardiac expression of BNP

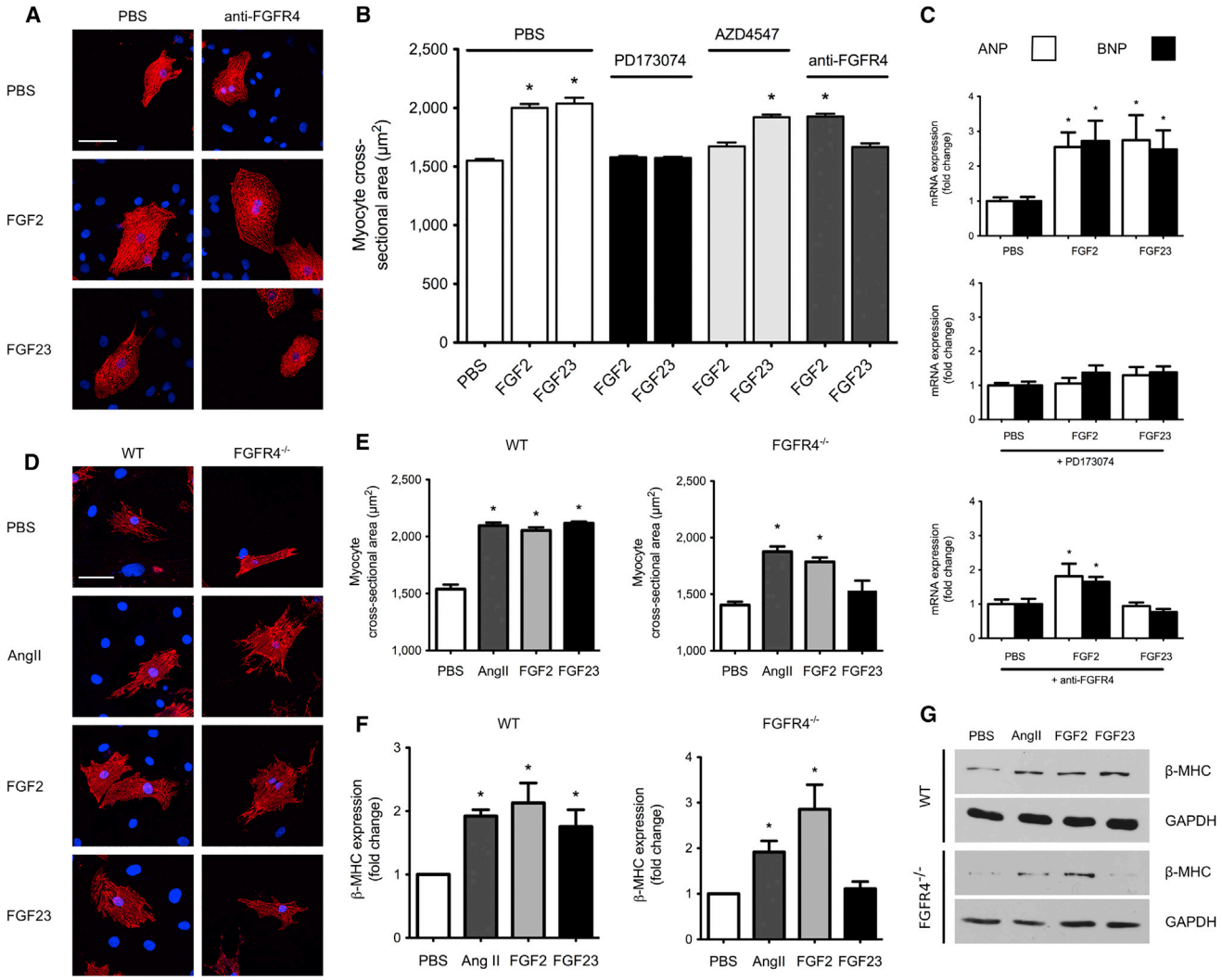

Figure 4. FGF23-Mediated Hypertrophic Growth of Isolated Cardiac Myocytes Requires FGFR4

(A) Immunofluorescence confocal images of isolated NRVM that were co-treated with FGF2 or FGF23 and anti-FGFR4 for 48 hr. Myocytes are labeled with anti-α-actinin (red), and DAPI (blue) identifies nuclei (original magnification, ×63; scale bar, 50 μm). NRVM treated with FGF23 or FGF2 appear larger than PBS-treated control cells. Anti-FGFR4 blocks the effect of FGF23, but not FGF2.

(B) Compared with PBS-treated control cells, 48 hr of treatment with FGF23 or FGF2 significantly increases cross-sectional area of isolated NRVM (mean ± SEM). Co-treatment with the pan-FGFR inhibitor, PD173074, prevents any increase in area regardless of the FGF. Inhibition of FGFR1–3 by AZD4547 prevents FGF2-induced, but not FGF23-induced, hypertrophy. An FGFR4-specific blocking antibody (anti-FGFR4) prevents FGF23-induced, but not FGF2-induced, hypertrophy (150 cells per condition; n = 3 independent isolations of NRVM; *p < 0.0001 compared with vehicle).

(C) Quantitative PCR analysis of NRVM 48 hr after co-treatment with FGF2 or FGF23 with PD173074 or anti-FGFR4. ANP and BNP expression are significantly elevated in FGF2- and FGF23-treated cells. PD173074 blocks the effects of both FGF2 and FGF23, but anti-FGFR4 blocks only the effects of FGF23 (n = 3 independent isolations of NRVM; *p < 0.05 compared with vehicle).

(D) Immunofluorescence confocal images of NMVM isolated from wild-type or *FGFR4*$^{-/-}$ mice that were treated with FGF2, FGF23, or AngII. Myocytes are labeled with anti-α-actinin (red), and DAPI (blue) identifies nuclei (original magnification, ×63; scale bar, 50 μm). Wild-type NMVM treated with FGF23, FGF2, or AngII appear larger than PBS-treated control cells. *FGFR4*$^{-/-}$ NMVM increase in size in response to FGF2 and AngII, but are protected from the effect of FGF23.

(E) FGF23, FGF2, and AngII induce significant increases in cross-sectional area of wild-type NMVM, but only FGF2 and AngII increase the size of NMVM isolated from *FGFR4*$^{-/-}$ mice (150 cells per condition; n = 3 independent isolations of NMVM; *p < 0.01 compared with vehicle).

(F) NMVM were treated with FGF23, FGF2, or AngII for 48 hr followed by immunoblot analysis with anti-β-MHC and anti-GAPDH, and signal quantification by densitometry. FGF23 induces increased β-MHC expression in wild-type, but not *FGFR4*$^{-/-}$, NMVM, whereas FGF2 and AngII increase β-MHC in NMVM of both genotypes (values represent fold change ± SEM compared with vehicle-treated cells; n = 4 independent isolations of NMVM; *p < 0.05).

(G) Representative immunoblots for the quantification presented in (F). GAPDH shows equal protein loading. See also Figure S4.

(Figures 7A–7D and 7F). *FGFR4Arg/Arg385* mice did not show increased content of myocardial collagen fiber (Figures 7B and 7E), but expression levels of some fibrotic markers were significantly elevated (Figure 7G). Echocardiography revealed that compared to control mice, *FGFR4Arg/Arg385* mice had significantly increased systolic ejection fraction and relative LV wall

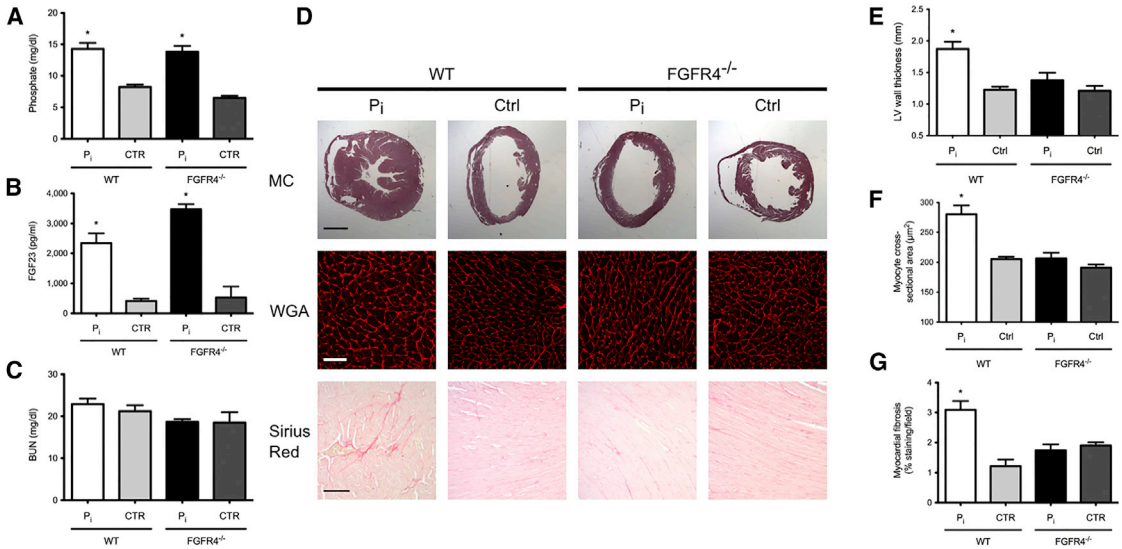

Figure 5. Diet-Induced Elevation of Serum FGF23 Does Not Result in LVH in *FGFR4*$^{-/-}$ Mice

(A–C) Compared to normal chow (Ctrl), high phosphate diet (P_i) significantly increases serum phosphate (A) and FGF23 (B) levels in wild-type (WT) and constitutive FGFR4 knockout (*FGFR4*$^{-/-}$) mice, but does not affect blood urea nitrogen (BUN) levels (C).

(D) Representative gross pathology of mid-chamber (MC) sections of the heart (H&E stain; original magnification, ×5; scale bar, 2 mm) and wheat germ agglutinin (WGA)-stained sections (original magnification, ×63; scale bar, 50 μm) demonstrate LVH, and picrosirius red stainings (original magnification, ×10; scale bar, 100 μm) show myocardial fibrosis in wild-type mice on high phosphate diet. *FGFR4*$^{-/-}$ mice on high phosphate or wild-type and *FGFR4*$^{-/-}$ mice on normal diet do not develop LVH or fibrosis.

(E–G) Wild-type mice on high phosphate diet develop significant increases in left ventricular (LV) wall thickness (E), cross-sectional area of individual cardiac myocytes (F), and myocardial deposition of collagen fibers (G), which do not occur in *FGFR4*$^{-/-}$ mice on high phosphate diet or wild-type and *FGFR4*$^{-/-}$ mice on normal diet.

All values are mean ± SEM (n = 4–11 mice per group; n = 100 cells per group for WGA analysis; *p < 0.001 compared with mice form the same genotype on normal chow). See also Figure S5.

thickness, and a trend toward diastolic dysfunction (p = 0.06; Figures 7H–7J). Interestingly, serum FGF23 levels were significantly increased in *FGFR4Arg/Arg385* compared to *FGFR4Gly/Gly385* mice (Figure 7K), but there was no relationship between FGF23 levels and LV wall thickness (r^2 = 0.01; p = 0.67). Thus, expression of a constitutively active FGFR4 variant is sufficient to induce LVH in mice, independently of FGF23 levels.

FGFR4Arg385 activated NFAT in the mouse heart, marked by elevated RCAN1 expression in cardiac extracts from *FGFR4Arg/Arg385* versus *FGFR4Gly/Gly385* mice (Figures S5E and S5F). We overexpressed V5-tagged *FGFR4Arg385* in HEK293 cells for 2 days followed by treatment with FGF23 or solvent for 30 min. In the absence of FGF23, cells expressing *FGFR4Arg385* showed increased phosphorylation of PLCγ and expression of the RCAN isoforms 1–4 (Figure S7). Treatment of *FGFR4Arg385* cells with FGF23 further increased phospho-PLCγ levels (Figure S7), whereas neither the presence of *FGFR4Arg385* nor treatment with FGF23 induced ERK1/2 phosphorylation. This is consistent with findings in mitotic cells, in which *FGFR4Arg385* induces proliferation, but does not activate Ras/MAPK signaling (Ezzat et al., 2013; Seitzer et al., 2010). As we have shown for α-klotho-independent, FGF23-mediated activation of wild-type FGFR4, we conclude that the glycine-to-arginine substitution at codon 385 of murine FGFR4 constitutively activates PLCγ/calcineurin/NFAT signaling, which might underlie the LVH phenotype observed in *FGFR4Arg/Arg385* knockin mice.

DISCUSSION

We report several findings that advance our understanding of FGF23, FGFR, and klotho biology. We demonstrate that FGFR4 is the cardiac receptor for FGF23 and that FGF23 can activate FGFR4 in cardiac myocytes in the absence of its co-receptor in the kidney, α-klotho. Unlike most reported FGF-FGFR interactions that stimulate phosphorylation of FRS2α or FRS2β and activate Ras/MAPK signaling (Eswarakumar et al., 2005), we provide direct evidence that FGFR4 binding by FGF23 activates the PLCγ/calcineurin/NFAT signaling axis, which is known to be a potent inducer of LVH in response to other pathological stimuli (Wilkins et al., 2004).

In addition to FGF23-induced hypertrophic growth of cardiac myocytes, FGFR4-induced PLCγ activation might function as a general pathway that mediates other non-mitogenic effects of specific FGF ligands. Indeed, previous studies showed that autophosphorylation of the PLCγ docking site of FGFR1 and consequent PLCγ activation is not required for the FGF-induced mitogenic response, but is essential for other FGF-regulated functions (Mohammadi et al., 1992; Peters et al., 1992; Sorokin et al., 1994). Since Ras/MAPK signaling is the major pathway of FGF-mediated mitogenic effects, but FGFR4 seems to primarily activate PLCγ (Shaoul et al., 1995; Vainikka et al., 1994), it is likely that FGFR4 activation does not induce cell proliferation, as supported by the much weaker mitogenic response of cells that express FGFR4 compared to FGFR1 or FGFR2 (Ornitz

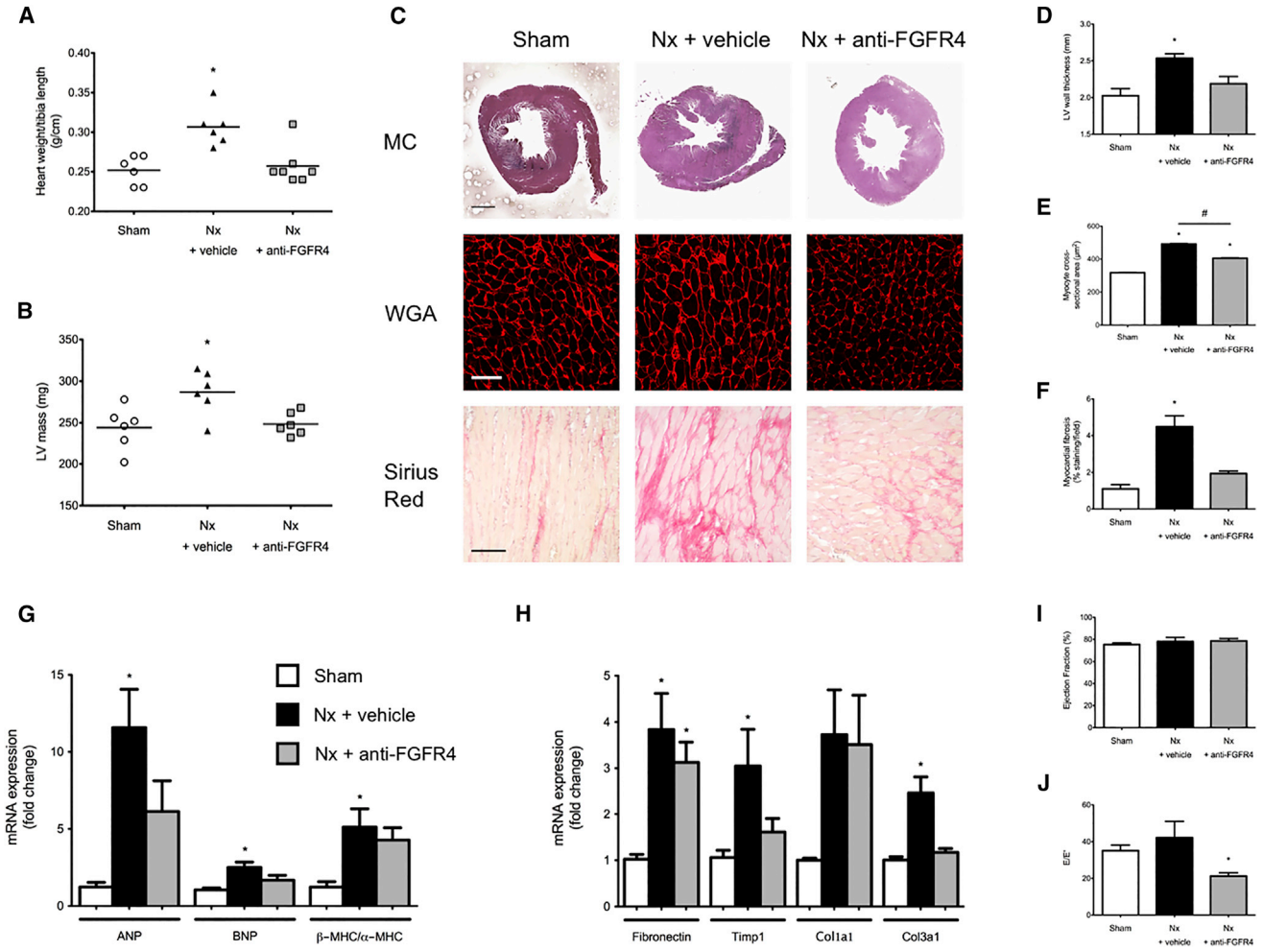

Figure 6. Pharmacological Inhibition of FGFR4 Attenuates LVH in a Rat Model of CKD

(A and B) Compared with sham nephrectomy, 5/6 nephrectomy (Nx) in rats results in increased ratio of heart weight to tibia length (A) and increased left ventricular mass (LVM) by echocardiography (B) at day 14 post-surgery. Each of these effects is attenuated by administering an FGFR4-specific blocking antibody (anti-FGFR4) (*$p < 0.05$ compared with Sham).

(C) Representative gross pathology sections (H&E stain; original magnification, ×2.5; scale bar, 2 mm), wheat germ agglutinin (WGA)-stained sections (original magnification, ×63; scale bar, 50 μm), and picrosirius red stainings (original magnification, ×10; scale bar, 100 μm) from the left ventricular mid-chamber (MC) at day 14 after 5/6 nephrectomy.

(D–F) Compared with vehicle, anti-FGFR4 attenuates the effects of 5/6 nephrectomy to increase left ventricular (LV) wall thickness (by gross pathology, (D), cross-sectional area of individual cardiac myocytes (E), and myocardial fibrosis (F). All values are mean ± SEM (n = 6–14 rats per group; *$p < 0.001$ compared with Sham; #$p < 0.01$ compared with 5/6 nephrectomy treated with vehicle).

(G and H) Quantitative PCR analysis of cardiac tissue shows that expression levels of hypertrophic markers (ANP, BNP, and β-MHC) (G) and of some fibrotic markers (TIMP metallopeptidase inhibitor 1, Timp1; collagen type 1 alpha 1, Col1a1; collagen type 3 alpha 1, Col3a1) (H) are significantly elevated in 5/6 nephrectomy rats that were treated with vehicle, but not in anti-FGFR4 treated rats (n = 6 rats per group; *$p < 0.05$ compared with Sham).

(I and J) Echocardiography shows no significant differences in ejection fraction among the three groups (I), but anti-FGFR4 significantly improves diastolic function (E/E') in 5/6 nephrectomy rats compared to vehicle-treatment (J) (n = 6–8 rats per group; *$p < 0.05$ compared with vehicle-injected 5/6 nephrectomy). See also Figures S5 and S6.

et al., 1996). These findings might also explain why previous in vitro studies that assayed MAPK activity or cell proliferation as measures of FGFR activation failed to demonstrate activation of any FGFR by FGF23 in the absence of α-klotho (Kurosu et al., 2006; Urakawa et al., 2006; Zhang et al., 2006).

Compared to the other FGFR isoforms, FGFR4 also has weaker kinase activity that results in less pronounced autophosphorylation and weaker phosphorylation of PLCγ (Raffioni et al., 1999; Shaoul et al., 1995; Vainikka et al., 1992). This could explain why studies that assayed tyrosine phosphorylation of FGFR4 or PLCγ following FGF stimulation failed to show FGFR4 activation. Our results suggest that studying the interaction of FGFR4 and PLCγ by immunoprecipitation is a more sensitive approach to detect FGFR4 activation than assessing tyrosine phosphorylation of either protein.

Previous analyses of cardiac FGFR4 expression yielded contradictory results (Fon Tacer et al., 2010; Seitzer et al., 2010). By using isoform-specific FGFR4 antibodies and analyzing

tissue from constitutive *FGFR4*$^{-/-}$ mice as negative control, we provide strong evidence that the FGFR4 protein is present in murine and human hearts and most likely expressed only in myocytes versus other cardiac cell types. We further show that FGFR4 activation per se appears to be sufficient to induce cardiac remodeling, as suggested by spontaneous development of LVH independently of FGF23 levels in mice expressing constitutively active FGFR4. Based on these findings, we speculate that FGFR4 activation triggers a pro-hypertrophic signaling pathway in the heart that may also be operative in other forms of heart disease that feature aberrant ventricular remodeling.

Another aspect of this report is our finding that α-klotho acts not only as a co-receptor that enhances FGF23 binding to FGFRs, as previously thought (Urakawa et al., 2006), but also as a molecular switch that directly influences differential recruitment of distinct signaling cascades downstream of FGFR. Instead of inducing global FGF23 resistance, our results suggest that CKD and other pathologic states of α-klotho deficiency may promote a switch in FGF23-induced signaling that drives different cellular responses to FGF23 in cells that express FGFR4 but not α-klotho. Some of these effects may be ultimately maladaptive, for example, LVH. Furthermore, by demonstrating that specific FGFR4 blocking antibodies attenuate LVH in 5/6 nephrectomized rats, our results suggest that FGFR4 activation is a critical molecular mechanism underlying LVH in states of α-klotho deficiency and FGF23 excess (Faul et al., 2011; Hu et al., 2015).

Although FGF23 and FGF2 can both induce hypertrophic growth of cardiac myocytes, FGF23 does so primarily by stimulating PLCγ/calcineurin/NFAT signaling, whereas FGF2 activates the Ras/MAPK signaling axis (Faul et al., 2011). Our study indicates that the different FGFs activate distinct downstream signaling pathways by binding and activating different FGFR isoforms. We show that FGF23, but not FGF2, can activate FGFR4 on cardiac myocytes and that FGFR4 blockade or deletion inhibits hypertrophic effects of FGF23, but not of FGF2. Since cardiac myocytes express multiple FGFR isoforms, and FGFR1 serves as the primary FGF2 receptor in other cell types (Ornitz et al., 1996), we postulate that FGFR1 mediates the cardiac hypertrophic effects of FGF2. Further experimental analyses using FGFR1 loss-of-function approaches are needed to test this hypothesis. Interestingly, it has been recently shown that the cardiac myocyte-specific overexpression of a constitutively active mutant form of FGFR1 in mice causes cardiac hypertrophy (Cilvik et al., 2013). Combined with our gain-of-function model for FGFR4, we conclude that myocardial FGFR1 or FGFR4 activation is sufficient to induce LVH.

We also observed that rodents with elevated serum FGF23 levels but global loss of FGFR4 function are protected from developing cardiac fibrosis. Whether this finding is based on direct effects of FGF23 on cardiac fibroblasts or altered communication between cardiac myocytes and fibroblasts in the course of cardiac injury requires further study, for example, by generating and investigating mouse models that carry cardiac myocyte-specific or cardiac fibroblast-specific deletions of FGFR4.

In addition to its cell biology findings, this report also has important implications for drug development and future clinical management of patients with CKD. Previously, we reported that delivery of a pan-FGFR inhibitor could prevent development of LVH and reverse established LVH in rats with CKD (Di Marco et al., 2014; Faul et al., 2011). These proof-of-concept findings suggested a therapeutic paradigm to attenuate cardiovascular disease in patients with CKD, but toxicity of pan-FGFR inhibitors precludes this approach in humans (Yanochko et al., 2013). Similarly, monoclonal antibodies that neutralize FGF23 are likely to be of limited utility in CKD because complete abrogation of FGF23 effects causes severe hyperphosphatemia that results in diffuse vascular calcification and increased mortality (Shalhoub et al., 2012). Our results suggest that it may be possible to selectively target FGFR4 to block the toxic effects of FGF23 in the heart without interfering with the essential effects of FGF23 to regulate phosphate homeostasis. Furthermore, whether FGFR4 activation mediates other adverse effects of elevated FGF23 levels in patients with CKD that could also be attenuated by selective FGFR4 blockade requires further study.

EXPERIMENTAL PROCEDURES

Study Approval

All animal protocols and experimental procedures were approved by the Institutional Animal Care and Use Committees at the University of Miami Miller School of Medicine (high-phosphate diet in wild-type and *FGFR4*$^{-/-}$ mice), the Max Planck Institute for Biochemistry in Martinsried (*FGFR4Arg385* knockin mouse), and the University of Münster (5/6 nephrectomy in rats). Autopsies and postmortem analyses of human tissue were approved by the medical ethics committee of the Hannover Medical School.

5/6 Nephrectomy Rat Model of CKD

Kidney disease was induced in Sprague Dawley rats using the 5/6 nephrectomy method (Di Marco et al., 2014). Rats were randomized to the following three groups of six animals each: sham nephrectomy, 5/6 nephrectomy plus intraperitoneal injections of vehicle (PBS), or 5/6 nephrectomy plus intraperitoneal injections of anti-FGFR4 blocking antibody (human monoclonal, U3-11; U3Pharma) at 25 mg/kg/day every 3 days beginning 1 hr after surgery. Fourteen days after surgery, echocardiography and blood pressure measurements were performed, animals were sacrificed, and the hearts were isolated and prepared for histological and serological analyses.

High Phosphate Diet in *FGFR4*$^{-/-}$ Mice

Five 6-month-old constitutive *FGFR4*$^{-/-}$ mice on the C57BL/6 background (Weinstein et al., 1998) and 11 wild-type littermates were switched from normal chow to a 2.0% phosphate diet (Teklad 08020, Harlan) for 12 weeks. Four 9-month-old wild-type and four *FGFR4*$^{-/-}$ mice that were maintained on a regular diet served as negative controls. Animals were sacrificed and the hearts were isolated, perfused ex vivo (6 ml of 10% formalin with 4 ml of 20 mM KCl), stored overnight in 10% formalin for fixation, and then serially sectioned (7-μm slices) and stained with H&E.

FGFR4Arg385 Knockin Mice

FGFR4Arg385 knockin mice on the C57BL/6 background were generated (Seitzer et al., 2010). Homozygous *FGFR4Arg/Arg385* male and female mice were analyzed, and wild-type littermates (*FGFR4Gly/Gly385*) served as negative controls. Nine to twelve animals per group were sacrificed at 6 months of age, and the hearts were isolated and prepared using the same protocol as described above.

Morphology, Fluorescence Microscopy, and Morphometry of Mouse and Rat Hearts

Short-axis heart sections were stained with H&E (VWR) and used to quantify myocardial thickness by measuring the distance from the inner to the outer myocardial edges at the mid-chamber zone. Mean left ventricular free wall thickness was calculated from seven measurements of wall thickness taken at 0, 30, 60, 90, 120, 150, and 180 degrees along the hemi-circle of the short

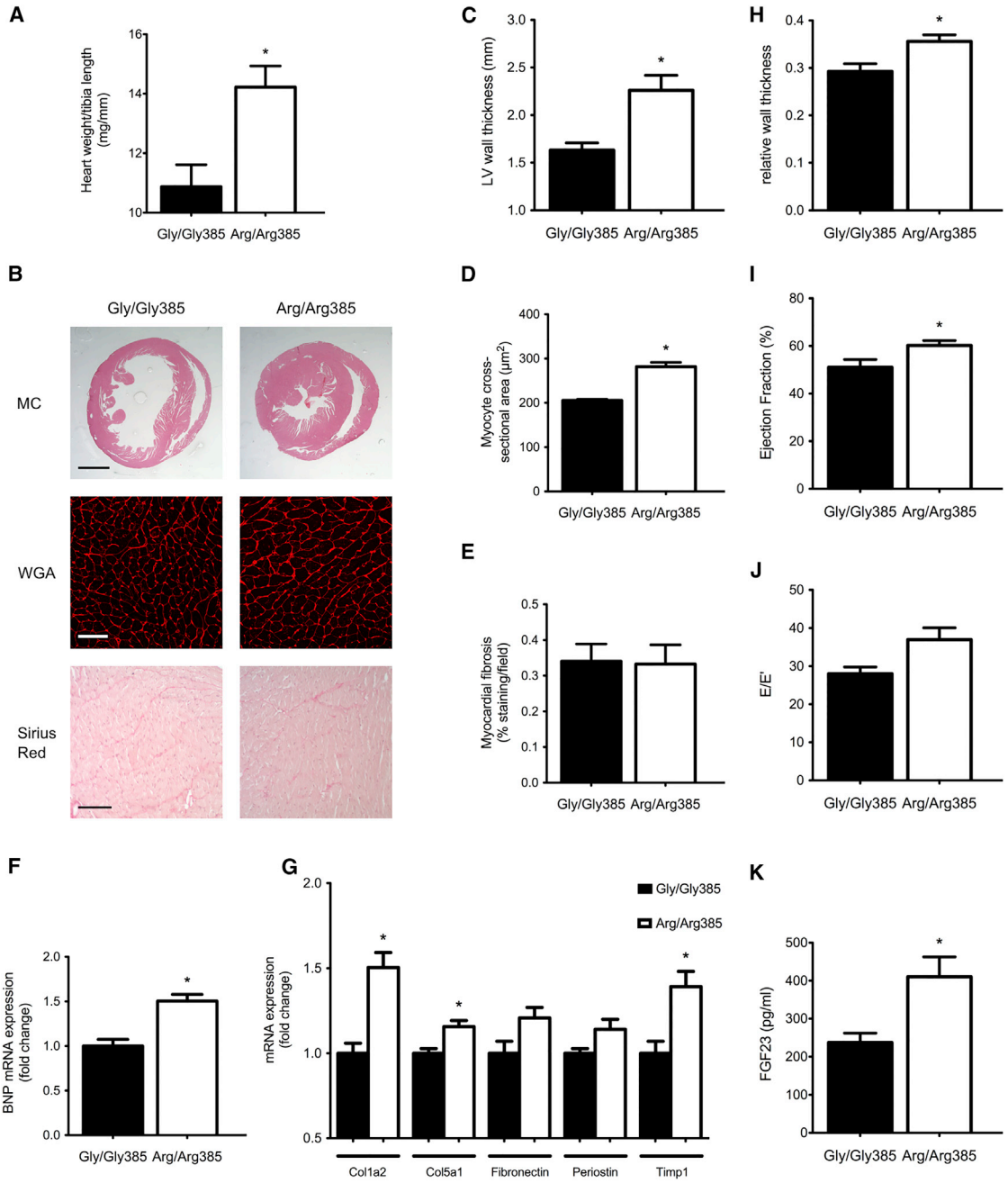

Figure 7. Knockin Mice with an FGFR4 Gain-of-Function Mutation Spontaneously Develop LVH

(A) Six-month old homozygous knockin mice carrying the Arg385 substitution in FGFR4 (*FGFR4Arg/Arg385*) manifest significant increases in the ratio of heart weight to tibia length compared with wild-type littermates (*FGFR4Gly/Gly385*) (mean ± SEM; n = 9–12 mice per group; *p < 0.01).

(B) Representative gross pathology of mid-chamber (MC) sections of the heart (H&E stain; original magnification, ×5; scale bar, 2 mm) and wheat germ agglutinin (WGA)-stained sections (original magnification, ×63; scale bar, 50 μm) demonstrate LVH in *FGFR4Arg/Arg385* mice but lack of myocardial fibrosis by picrosirius red staining (original magnification, ×100; scale bar, 100 μm).

(C–E) Compared with wild-type, *FGFR4Arg/Arg385* mice develop significant increases in left ventricular (LV) wall thickness (mean ± SEM; n = 9–12 mice per group; *p < 0.01) (C) and cross-sectional area of individual cardiac myocytes (mean ± SEM; n = 100 cells per group; *p < 0.0001) (D), but no difference in collagen deposition (mean ± SEM; n = 9–12 mice per group) (E).

(F) Quantitative PCR analysis of total hearts from mice reveals significantly elevated BNP expression in 6-month-old *FGFR4Arg/Arg385* mice compared with wild-type (n = 4–6 mice per group; *p < 0.01).

(G) Quantitative PCR analysis of cardiac tissue shows that expression levels of some fibrotic markers (TIMP metallopeptidase inhibitor 1, Timp1; collagen type 1 alpha 2, Col1a2; collagen type 5 alpha 1, Col5a1) are significantly elevated in *FGFR4Arg/Arg385* mice compared to wild-type mice (n = 6 mice per group; *p < 0.01).

(legend continued on next page)

axis of the free wall. Images were taken on a Nikon SMZ 1500 microscope using 0.75× magnification.

We measured the cross-sectional area of individual cardiac myocytes in paraffin-embedded short-axis sections of mouse and rat hearts. Briefly, 7-μm-thick sections were deparaffinized according to our established protocols (Faul et al., 2011). To visualize cellular borders, fixed tissue was incubated with wheat germ agglutinin (WGA) conjugated to Alexa Fluor555 (Invitrogen) at 1 mg/ml in PBS containing 10 mM sodium azide. Immunofluorescence images were taken on a Leica TCS-SP5 confocal microscope with a 63× oil objective. Leica AF6000 fluorescence software was used to quantify cross-sectional area of 25 cells per field at 4 fields along the mid-chamber free wall based on WGA-positive staining.

Short-axis cardiac sections from mice and rats were stained with picrosirius red (Sigma-Aldrich) and used to quantify myocardial fibrosis. Sections were deparaffinized, counterstained with hematoxylin (VWR), and incubated in picrosirius red solution for 60 min. After washing in acidified water, sections were dehydrated in ascending ethanol series and mounted in non-aqueous mounting media. For quantification of myocardial fibrosis, 10 images were taken around the complete left ventricle using an Olympus BX41 microscope with 10× magnification. Collagen content was determined by quantification of picrosirius-red-positive area per field of view using ImageJ software (NIH).

We analyzed RCAN1 expression in paraffin-embedded short-axis sections of mouse and rat hearts by immunoperoxidase staining. 7-μm-thick sections were deparaffinized and rehydrated, and antigen retrieval was performed using a citrate acid-based antigen unmasking solution (Vector Laboratories H-3300). After blocking endogenous peroxidase activity with 1% H_2O_2 for 20 min, non-specific sites were blocked with goat serum blocking solution (Sigma-Aldrich) for 1 hr. Sections were incubated in primary antibody (anti-RCAN1 at 1:50 [Harrison et al., 2004]) overnight and immunostained employing the avidin-biotin enzyme complex (ABC; Thermo Scientific) method. Reaction products were visualized by 3,3′-diaminobenzidine (DAB; Vector Laboratories). After dehydration in ascending alcohol, series sections were mounted and images were taken using an Olympus BX41 microscope with 10× magnification.

Echocardiography of Mouse and Rat Hearts

High-resolution echocardiography (15 MHz) in rats was performed at 14 days after surgery to assess LV mass, wall and chamber dimensions, and systolic and diastolic function using an HDI 5000 Ultrasound system (Philips). M-mode, 2D, and 3D recordings were obtained under general anesthesia delivered through a nose mask while heart rate and body temperature were maintained. Echocardiography in mice was conducted as described for rats. Relative wall thickness was estimated as [interventricular septum diastolic (IVSd) + LV posterior wall diastolic (LVPWd)]/LV diameter diastolic (LVDd).

Blood pressure was measured in conscious rats using a computerized rat-tail cuff technique (CODA, Kent Scientific).

Immunocytochemistry and Morphometry of Isolated Cardiac Myocytes

Cultured cardiac myocytes were fixed in 2% paraformaldehyde (PFA) (in 5 mg/ml sucrose) for 5 min and permeabilized in 1% Triton X-100 (in PBS) for 10 min. We analyzed hypertrophic growth of isolated NRVM and NMVM on laminin-coated glass coverslips after 48 hr of treatment with growth factors. For FGFR4 expression and localization analyses, untreated NMVM from wild-type and *FGFR4*$^{-/-}$ mice were immunolabeled. The mouse monoclonal antibody against sarcomeric α-actinin (EA-53; Sigma-Aldrich) was used at 1:1,000, and rabbit polyclonal anti-FGFR4 (C-16; Santa Cruz) at 1:50. Cy3-conjugated goat-anti mouse and Alexa488-conjugated goat-anti rabbit (Jackson ImmunoResearch) were used as secondary antibodies at 1:300. To visualize nuclei, fixed cells were incubated with 4',6-diamidino-2-phenylindole (DAPI; 400 ng/ml in PBS) for 10 min. Immunofluorescence images were taken on a Leica TCS-SP5 confocal microscope with a 63× oil objective.

Myocyte cross-sectional area was measured based on α-actinin-positive staining using Leica AF6000 fluorescence software. To assess the signaling pathways involved in FGF23- and FGF2-mediated hypertrophy, we analyzed the morphometry of plated cells that were pre-treated with specific inhibitors for 60 min prior to the addition of the FGFs at 25 ng/ml (NRVMs) or at 100 ng/ml (NMVMs). The following inhibitors and concentrations were used: pan-FGFR, PD173074 (Sigma Aldrich) at 10 nM (Mohammadi et al., 1998); FGFR1–3, AZD4547 (ChemieTek) at 5 nM (Gavine et al., 2012); and FGFR4 blocking antibody (human monoclonal, U3-11; U3Pharma) at 10 μg/ml.

Statistical Analysis of In Vitro and Animal Data

Data are presented as mean ± SEM. ANOVA and t tests were used for statistical inference with two-tailed p values < 0.05 considered significant. No statistical method was used, but extensive laboratory experience from previous publications was used to predetermine sample size. No formal randomization was used in any experiment; for in vivo experiments, animals were unbiasedly assigned into different treatment groups. Group allocation was not performed in a blinded manner. Whenever possible, experimenters were blinded to the groups (e.g., in immunofluorescence and immunohistochemistry experiments by hiding group designation and genotype of animals until after quantification and analysis). No animals or samples were excluded from data analysis.

SUPPLEMENTAL INFORMATION

Supplemental Information includes Supplemental Experimental Procedures, seven figures, and two tables and can be found with this article online at http://dx.doi.org/10.1016/j.cmet.2015.09.002.

AUTHOR CONTRIBUTIONS

A.G., A.P.A., and C.F. designed the study, performed experiments, and analyzed the data. K.S., S.S., A.S., and C.Y. were involved in performing in vitro studies and cDNA cloning. V.D. and A.M. were involved in measurements of mouse tibia length and serum FGF23 levels. J.L. and L.A.S. performed the flow cytometry analysis. G.S.D.M, D.K., S.R., A.B.M., H.P., J.S., and M.B designed, conducted, and analyzed the 5/6 nephrectomy study in rats. C.K., S.H., and N.F. performed in vitro analyses of NFAT-reporter cardiac myocytes. M.L.-N., B.R., and D.H. collected and analyzed human cardiac tissue. B.S. and A.U. provided the FGFR4Arg385 knockin mouse model, collected serum and hearts, and conducted expression analysis. R.A. and B.A. generated and characterized the anti-FGFR4 blocking antibody. M.W., A.F., J.M.H., M.B., and A.U. were involved in the study design and data analysis. A.G., M.W., and C.F. wrote the paper. A.G. and A.P.A. contributed equally to the study.

CONFLICTS OF INTEREST

The authors declare competing financial interests: M.W. has served as a consultant or received honoraria from Amgen, Keryx, Lutipold, Opko, Pfizer, and Sanofi. R.A. and J.B. are employees of U3 Pharma GmbH, Germany. A.G. was supported by Roche, A.U. by Daiichi-Sankyo, and C.F. by U3 Pharma GmbH, Germany. A.F. is an inventor on pending patents aimed to diagnose or treat proteinuric renal diseases and stands to gain royalties from their future commercialization. A.F. is a consultant for Hoffman-La Roche, Genentech, Janssen, Mesoblast, Abbvie, Boehringer Ingelheim, Alexion, Bristol Meyer Squibb, and Pfizer.

ACKNOWLEDGMENTS

This study was supported by the Stifterverband für die Deutsche Wissenschaft and Simon-Claussen-Stiftung (H1405409999915626 to M.B.), the Deutsche

(H–J) Echocardiography shows that compared to wild-type mice, relative wall thickness (H), ejection fraction (I) and diastolic dysfunction (E/E') (J) are increased in *FGFR4Arg/Arg385* mice (n = 5–9 mice per group; *p < 0.05).

(K) *FGFR4Arg/Arg385* mice demonstrate increased serum FGF23 levels compared with wild-type littermates (mean ± SEM; n = 9–12 mice per group; *p < 0.05). See also Figures S5 and S7.

Forschungs Gemeinschaft (GR 4228/1-1 to A.G. and SFB656 C7 to S.R.), Roche (A.G.), the Max Planck Society (A.U.), Daiichi-Sankyo (A.U.), State of Florida (3KN05) and Florida Heart Research Institute (L.A.S.), the Starr Foundation (J.M.H.), the American Heart Association (A.G., M.W., and C.F.), the American Society of Nephrology (C.F.), U3 Pharma GmbH, Germany (C.F.), and grants F30DK091057 (A.P.A.), F31DK10236101 (K.S.), F31DK09566101 (A.S.), R01DK090316 (A.F.), R01DK104753 (A.F.), K01AG040468 (L.A.S.), R01HL110737 (J.M.H.), R01HL094849 (J.M.H.), R01HL107110 (J.M.H.), R01HL084275 (J.M.H.), R01DK076116 (M.W.), K24DK093723 (M.W.), and R01HL128714 (C.F.) from NIH. Gabriel Gaidosh (University of Miami Miller School of Medicine) assisted with confocal microscopy, and Johannes Backs (University of Heidelberg) with establishing the neonatal mouse ventricular myocyte cultures. Makoto Kuro-o (University of Texas Southwestern) provided FGFR and klotho cDNA constructs, Timothy McKinsey (University of Colorado) the anti-RCAN1 antibody, and Thomas Mariani (University of Rochester Medical Center) the global FGFR4 knockout mouse line.

Received: January 23, 2015
Revised: July 1, 2015
Accepted: September 1, 2015
Published: October 1, 2015

REFERENCES

Bange, J., Prechtl, D., Cheburkin, Y., Specht, K., Harbeck, N., Schmitt, M., Knyazeva, T., Müller, S., Gärtner, S., Sures, I., et al. (2002). Cancer progression and tumor cell motility are associated with the FGFR4 Arg(388) allele. Cancer Res. *62*, 840–847.

Burgess, W.H., Dionne, C.A., Kaplow, J., Mudd, R., Friesel, R., Zilberstein, A., Schlessinger, J., and Jaye, M. (1990). Characterization and cDNA cloning of phospholipase C-gamma, a major substrate for heparin-binding growth factor 1 (acidic fibroblast growth factor)-activated tyrosine kinase. Mol. Cell. Biol. *10*, 4770–4777.

Cilvik, S.N., Wang, J.I., Lavine, K.J., Uchida, K., Castro, A., Gierasch, C.M., Weinheimer, C.J., House, S.L., Kovacs, A., Nichols, C.G., and Ornitz, D.M. (2013). Fibroblast growth factor receptor 1 signaling in adult cardiomyocytes increases contractility and results in a hypertrophic cardiomyopathy. PLoS ONE *8*, e82979.

de Simone, G., Gottdiener, J.S., Chinali, M., and Maurer, M.S. (2008). Left ventricular mass predicts heart failure not related to previous myocardial infarction: the Cardiovascular Health Study. Eur. Heart J. *29*, 741–747.

Di Marco, G.S., Reuter, S., Kentrup, D., Grabner, A., Amaral, A.P., Fobker, M., Stypmann, J., Pavenstädt, H., Wolf, M., Faul, C., and Brand, M. (2014). Treatment of established left ventricular hypertrophy with fibroblast growth factor receptor blockade in an animal model of CKD. Nephrol. Dial. Transplant. *29*, 2028–2035.

Eckardt, K.U., Coresh, J., Devuyst, O., Johnson, R.J., Köttgen, A., Levey, A.S., and Levin, A. (2013). Evolving importance of kidney disease: from subspecialty to global health burden. Lancet *382*, 158–169.

Eswarakumar, V.P., Lax, I., and Schlessinger, J. (2005). Cellular signaling by fibroblast growth factor receptors. Cytokine Growth Factor Rev. *16*, 139–149.

Ezzat, S., Zheng, L., Florez, J.C., Stefan, N., Mayr, T., Hliang, M.M., Jablonski, K., Harden, M., Stančáková, A., Laakso, M., et al. (2013). The cancer-associated FGFR4-G388R polymorphism enhances pancreatic insulin secretion and modifies the risk of diabetes. Cell Metab. *17*, 929–940.

Faul, C., Amaral, A.P., Oskouei, B., Hu, M.C., Sloan, A., Isakova, T., Gutiérrez, O.M., Aguillon-Prada, R., Lincoln, J., Hare, J.M., et al. (2011). FGF23 induces left ventricular hypertrophy. J. Clin. Invest. *121*, 4393–4408.

Fon Tacer, K., Bookout, A.L., Ding, X., Kurosu, H., John, G.B., Wang, L., Goetz, R., Mohammadi, M., Kuro-o, M., Mangelsdorf, D.J., and Kliewer, S.A. (2010). Research resource: Comprehensive expression atlas of the fibroblast growth factor system in adult mouse. Mol. Endocrinol. *24*, 2050–2064.

Gavine, P.R., Mooney, L., Kilgour, E., Thomas, A.P., Al-Kadhimi, K., Beck, S., Rooney, C., Coleman, T., Baker, D., Mellor, M.J., et al. (2012). AZD4547: an orally bioavailable, potent, and selective inhibitor of the fibroblast growth factor receptor tyrosine kinase family. Cancer Res. *72*, 2045–2056.

Goetz, R., Ohnishi, M., Kir, S., Kurosu, H., Wang, L., Pastor, J., Ma, J., Gai, W., Kuro-o, M., Razzaque, M.S., and Mohammadi, M. (2012). Conversion of a paracrine fibroblast growth factor into an endocrine fibroblast growth factor. J. Biol. Chem. *287*, 29134–29146.

Gutiérrez, O.M., Mannstadt, M., Isakova, T., Rauh-Hain, J.A., Tamez, H., Shah, A., Smith, K., Lee, H., Thadhani, R., Jüppner, H., and Wolf, M. (2008). Fibroblast growth factor 23 and mortality among patients undergoing hemodialysis. N. Engl. J. Med. *359*, 584–592.

Gutiérrez, O.M., Januzzi, J.L., Isakova, T., Laliberte, K., Smith, K., Collerone, G., Sarwar, A., Hoffmann, U., Coglianese, E., Christenson, R., et al. (2009). Fibroblast growth factor 23 and left ventricular hypertrophy in chronic kidney disease. Circulation *119*, 2545–2552.

Harrison, B.C., Roberts, C.R., Hood, D.B., Sweeney, M., Gould, J.M., Bush, E.W., and McKinsey, T.A. (2004). The CRM1 nuclear export receptor controls pathological cardiac gene expression. Mol. Cell. Biol. *24*, 10636–10649.

Hu, M.C., Shi, M., Cho, H.J., Adams-Huet, B., Paek, J., Hill, K., Shelton, J., Amaral, A.P., Faul, C., Taniguchi, M., et al. (2015). Klotho and phosphate are modulators of pathologic uremic cardiac remodeling. J. Am. Soc. Nephrol. *26*, 1290–1302.

Isakova, T., Xie, H., Yang, W., Xie, D., Anderson, A.H., Scialla, J., Wahl, P., Gutiérrez, O.M., Steigerwalt, S., He, J., et al.; Chronic Renal Insufficiency Cohort (CRIC) Study Group (2011). Fibroblast growth factor 23 and risks of mortality and end-stage renal disease in patients with chronic kidney disease. JAMA *305*, 2432–2439.

Izumo, S., Lompré, A.M., Matsuoka, R., Koren, G., Schwartz, K., Nadal-Ginard, B., and Mahdavi, V. (1987). Myosin heavy chain messenger RNA and protein isoform transitions during cardiac hypertrophy. Interaction between hemodynamic and thyroid hormone-induced signals. J. Clin. Invest. *79*, 970–977.

Kurosu, H., Ogawa, Y., Miyoshi, M., Yamamoto, M., Nandi, A., Rosenblatt, K.P., Baum, M.G., Schiavi, S., Hu, M.C., Moe, O.W., and Kuro-o, M. (2006). Regulation of fibroblast growth factor-23 signaling by klotho. J. Biol. Chem. *281*, 6120–6123.

Mohammadi, M., Honegger, A.M., Rotin, D., Fischer, R., Bellot, F., Li, W., Dionne, C.A., Jaye, M., Rubinstein, M., and Schlessinger, J. (1991). A tyrosine-phosphorylated carboxy-terminal peptide of the fibroblast growth factor receptor (Flg) is a binding site for the SH2 domain of phospholipase C-gamma 1. Mol. Cell. Biol. *11*, 5068–5078.

Mohammadi, M., Dionne, C.A., Li, W., Li, N., Spivak, T., Honegger, A.M., Jaye, M., and Schlessinger, J. (1992). Point mutation in FGF receptor eliminates phosphatidylinositol hydrolysis without affecting mitogenesis. Nature *358*, 681–684.

Mohammadi, M., Froum, S., Hamby, J.M., Schroeder, M.C., Panek, R.L., Lu, G.H., Eliseenkova, A.V., Green, D., Schlessinger, J., and Hubbard, S.R. (1998). Crystal structure of an angiogenesis inhibitor bound to the FGF receptor tyrosine kinase domain. EMBO J. *17*, 5896–5904.

Molkentin, J.D., Lu, J.R., Antos, C.L., Markham, B., Richardson, J., Robbins, J., Grant, S.R., and Olson, E.N. (1998). A calcineurin-dependent transcriptional pathway for cardiac hypertrophy. Cell *93*, 215–228.

Ogawa, Y., Kurosu, H., Yamamoto, M., Nandi, A., Rosenblatt, K.P., Goetz, R., Eliseenkova, A.V., Mohammadi, M., and Kuro-o, M. (2007). BetaKlotho is required for metabolic activity of fibroblast growth factor 21. Proc. Natl. Acad. Sci. USA *104*, 7432–7437.

Ornitz, D.M., and Itoh, N. (2001). Fibroblast growth factors. Genome Biol. *2*, reviews3005.1–reviews3005.12.

Ornitz, D.M., Xu, J., Colvin, J.S., McEwen, D.G., MacArthur, C.A., Coulier, F., Gao, G., and Goldfarb, M. (1996). Receptor specificity of the fibroblast growth factor family. J. Biol. Chem. *271*, 15292–15297.

Partanen, J., Mäkelä, T.P., Eerola, E., Korhonen, J., Hirvonen, H., Claesson-Welsh, L., and Alitalo, K. (1991). FGFR-4, a novel acidic fibroblast growth factor receptor with a distinct expression pattern. EMBO J. *10*, 1347–1354.

Peters, K.G., Marie, J., Wilson, E., Ives, H.E., Escobedo, J., Del Rosario, M., Mirda, D., and Williams, L.T. (1992). Point mutation of an FGF receptor

abolishes phosphatidylinositol turnover and Ca2+ flux but not mitogenesis. Nature *358*, 678–681.

Raffioni, S., Thomas, D., Foehr, E.D., Thompson, L.M., and Bradshaw, R.A. (1999). Comparison of the intracellular signaling responses by three chimeric fibroblast growth factor receptors in PC12 cells. Proc. Natl. Acad. Sci. USA *96*, 7178–7183.

Seitzer, N., Mayr, T., Streit, S., and Ullrich, A. (2010). A single nucleotide change in the mouse genome accelerates breast cancer progression. Cancer Res. *70*, 802–812.

Shalhoub, V., Shatzen, E.M., Ward, S.C., Davis, J., Stevens, J., Bi, V., Renshaw, L., Hawkins, N., Wang, W., Chen, C., et al. (2012). FGF23 neutralization improves chronic kidney disease-associated hyperparathyroidism yet increases mortality. J. Clin. Invest. *122*, 2543–2553.

Shaoul, E., Reich-Slotky, R., Berman, B., and Ron, D. (1995). Fibroblast growth factor receptors display both common and distinct signaling pathways. Oncogene *10*, 1553–1561.

Sorokin, A., Mohammadi, M., Huang, J., and Schlessinger, J. (1994). Internalization of fibroblast growth factor receptor is inhibited by a point mutation at tyrosine 766. J. Biol. Chem. *269*, 17056–17061.

Urakawa, I., Yamazaki, Y., Shimada, T., Iijima, K., Hasegawa, H., Okawa, K., Fujita, T., Fukumoto, S., and Yamashita, T. (2006). Klotho converts canonical FGF receptor into a specific receptor for FGF23. Nature *444*, 770–774.

Vainikka, S., Partanen, J., Bellosta, P., Coulier, F., Birnbaum, D., Basilico, C., Jaye, M., and Alitalo, K. (1992). Fibroblast growth factor receptor-4 shows novel features in genomic structure, ligand binding and signal transduction. EMBO J. *11*, 4273–4280.

Vainikka, S., Joukov, V., Wennström, S., Bergman, M., Pelicci, P.G., and Alitalo, K. (1994). Signal transduction by fibroblast growth factor receptor-4 (FGFR-4). Comparison with FGFR-1. J. Biol. Chem. *269*, 18320–18326.

Wang, J., Yu, W., Cai, Y., Ren, C., and Ittmann, M.M. (2008). Altered fibroblast growth factor receptor 4 stability promotes prostate cancer progression. Neoplasia *10*, 847–856.

Weinstein, M., Xu, X., Ohyama, K., and Deng, C.X. (1998). FGFR-3 and FGFR-4 function cooperatively to direct alveogenesis in the murine lung. Development *125*, 3615–3623.

Wilkins, B.J., Dai, Y.S., Bueno, O.F., Parsons, S.A., Xu, J., Plank, D.M., Jones, F., Kimball, T.R., and Molkentin, J.D. (2004). Calcineurin/NFAT coupling participates in pathological, but not physiological, cardiac hypertrophy. Circ. Res. *94*, 110–118.

Wolf, M. (2012). Update on fibroblast growth factor 23 in chronic kidney disease. Kidney Int. *82*, 737–747.

Yang, J., Rothermel, B., Vega, R.B., Frey, N., McKinsey, T.A., Olson, E.N., Bassel-Duby, R., and Williams, R.S. (2000). Independent signals control expression of the calcineurin inhibitory proteins MCIP1 and MCIP2 in striated muscles. Circ. Res. *87*, E61–E68.

Yanochko, G.M., Vitsky, A., Heyen, J.R., Hirakawa, B., Lam, J.L., May, J., Nichols, T., Sace, F., Trajkovic, D., and Blasi, E. (2013). Pan-FGFR inhibition leads to blockade of FGF23 signaling, soft tissue mineralization, and cardiovascular dysfunction. Toxicol. Sci. *135*, 451–464.

Zhang, X., Ibrahimi, O.A., Olsen, S.K., Umemori, H., Mohammadi, M., and Ornitz, D.M. (2006). Receptor specificity of the fibroblast growth factor family. The complete mammalian FGF family. J. Biol. Chem. *281*, 15694–15700.